THE JOURNAL OF BIOLOGICAL CHEMISTRY
Vol. 278, No. 46, Issue of November 14, pp. 45937–45945, 2003
Printed in U.S.A.

Structural Insights and Biological Effects of Glycogen Synthase Kinase 3-specific Inhibitor AR-A014418*

Received for publication, June 13, 2003, and in revised form, August 14, 2003
Published, JBC Papers in Press, August 19, 2003, DOI 10.1074/jbc.M306268200

Ratan Bhat‡§, Yafeng Xue¶, Stefan Berg‡, Sven Hellberg‡, Mats Ormö¶, Yvonne Nilsson‡, Ann-Cathrin Radesäter‡, Eva Jerning‡, Per-Olof Markgren‡, Thomas Borgegård‡, Martin Nylöf‡, Alfredo Giménez-Cassina‖, Félix Hernández‖**, Jose J. Lucas‖**, Javier Díaz-Nido‖**, and Jesús Avila‖****

From ‡AstraZeneca R&D, 15185 Södertälje, Sweden, ¶AstraZeneca R&D, 43183 Mölndal, Sweden, and the ‖Centro de Biología Molecular "Severo Ochoa," Consejo Superior de Investigaciones Científicas, Universidad Autónoma de Madrid, 28049 Madrid, Spain

Glycogen synthase kinase 3 (GSK3) is a serine/threonine kinase that has been implicated in pathological conditions such as diabetes and Alzheimer's disease. We report the characterization of a GSK3 inhibitor, AR-A014418, which inhibits GSK3 (IC_{50} = 104 ± 27 nM), in an ATP-competitive manner (K_i = 38 nM). AR-A014418 does not significantly inhibit cdk2 or cdk5 (IC_{50} > 100 μM) or 26 other kinases demonstrating high specificity for GSK3. We report the co-crystallization of AR-A014418 with the GSK3β protein and provide a description of the interactions within the ATP pocket, as well as an understanding of the structural basis for the selectivity of AR-A014418. AR-A014418 inhibits tau phosphorylation at a GSK3-specific site (Ser-396) in cells stably expressing human four-repeat tau protein. AR-A014418 protects N2A neuroblastoma cells against cell death mediated by inhibition of the phosphatidylinositol 3-kinase/protein kinase B survival pathway. Furthermore, AR-A014418 inhibits neurodegeneration mediated by β-amyloid peptide in hippocampal slices. AR-A014418 may thus have important applications as a tool to elucidate the role of GSK3 in cellular signaling and possibly in Alzheimer's disease. AR-A014418 is the first compound of a family of specific inhibitors of GSK3 that does not significantly inhibit closely related kinases such as cdk2 or cdk5.

Alzheimer's disease (AD)[1] affects more than 18 million people worldwide. The onset is insidious, and the loss of memory is an early indicator of the disease. As the disease progresses, there are psychiatric abnormalities and motor deficits and death occurs within 7–8 years after diagnosis. The pathological hallmarks of AD include extracellular amyloid plaques and intraneuronal neurofibrillary tangles (NFTs) (1, 2). Neurodegeneration is also evident in the limbic regions of the brain, and brain atrophy occurs at the later stages. The density of NFTs correlates extremely well with the clinical severity of the disease, and the distribution follows a characteristic pattern of expansion as the disease progresses (3). This provides a compelling argument that strategies to inhibit factors leading to NFT development and neuronal death would be useful in the treatment of mid-moderate stage AD.

NFTs are found in the neuronal cell bodies and apical dendrites and comprise aggregates of paired helical filaments (PHFs), which are assembled from hyperphosphorylated forms of the microtubule-associated protein tau (4–6). Pathologic alterations in the microtubule-associated protein tau leading to PHFs and subsequently NFT have been implicated in a number of neurodegenerative disorders, particularly dementias, including AD, dementia pugilistic, progressive supranuclear palsy, frontotemporal dementia, and amyotrophic lateral sclerosis dementia (6).

GSK3β, also called tau phosphorylating kinase I (7), is a serine/threonine kinase that has highest abundance in brain and is localized primarily in neurons (8–10). It is highly conserved throughout evolution, and its expression is decreased in the adult (10). Aberrant increase in GSK3β expression and activity in adult brain has been directly linked to several of the key neuropathological mechanisms of AD (11, 12, 51). GSK3 has two major isoforms (α and β), which are 98% identical within the catalytic domain. GSK3 phosphorylates tau at most sites, which becomes abnormally hyperphosphorylated in PHFs, both in cells (13) and in rodents (14, 15), and has been linked to the production of β-amyloid, the chief constituent of amyloid plaques (51). The most crucial pathological link with AD has been its association with PHFs (16, 17).

GSK3 has also been linked to the downstream effects of β-amyloid. Exposure of cortical and hippocampal primary neuronal cultures to β-amyloid induces the activation of GSK3β (18) and cell death (19, 20). Blockade of GSK3β expression by antisense oligonucleotides (20) or its activity by lithium (21) inhibits Aβ-induced neurodegeneration of cortical and hippocampal primary cultures. Presenilin-1 (PS-1), a protein influencing APP metabolism and linked to familial AD, has been

* The costs of publication of this article were defrayed in part by the payment of page charges. This article must therefore be hereby marked "*advertisement*" in accordance with 18 U.S.C. Section 1734 solely to indicate this fact.

The atomic coordinates and structure factors (code 1Q5K) have been deposited in the Protein Data Bank, Research Collaboratory for Structural Bioinformatics, Rutgers University, New Brunswick, NJ (http://www.rcsb.org/).

§ To whom correspondence should be addressed: AstraZeneca R&D Södertälje, Research DMPK, Bldg. 231:213B, 15185 Södertälje, Sweden. Tel.: 46-8-553-29207; Fax: 46-8-553-21560; E-mail: ratan.bhat@astrazeneca.com.

** Supported by grants from the Comunidad de Madrid, the Fundación "La Caixa," the Lilly Foundation, the Spanish Comisión Interministerial de Ciencia y Tecnología, and an institutional grant from the Fundación Ramón Areces.

[1] The abbreviations used are: AD, Alzheimer's disease; NFT, intraneuronal neurofibrillary tangle; PHF, paired helical filament; GSK, glycogen synthase kinase; APP, amyloid precursor protein; DTT, dithiothreitol; PS, presenilin; GST, glutathione *S*-transferase; PI, propidium iodide; SPA, scintillation proximity assay; MOPS, 4-morpholinepropanesulfonic acid; BisTris, 2-[bis(2-hydroxyethyl)amino]-2-(hydroxymethyl)propane-1,3-diol; Aβ, amyloid β; PBS, phosphate-buffered saline; eIF2B, eukaryotic initiation factor 2B; PI3K, phosphatidylinositol 3-kinase; PKB, protein kinase B.

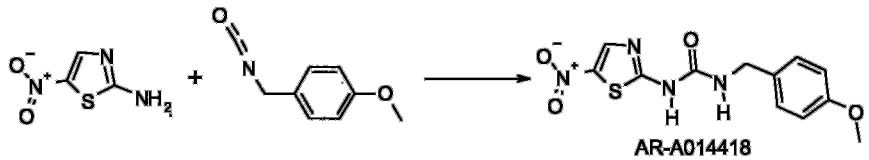

SCHEME I. **AR-A014418 synthesis.** Reagents and conditions were as follows: *N*,*N*-dimethylformamide, 100 °C, 15 h.

shown to directly bind GSK3β and tau in co-immunoprecipitation experiments from human brain samples (22). Thus, the ability of PS-1 to bring GSK3β and tau into close proximity suggests that PS-1 may regulate phosphorylation of tau by GSK3β. Mutant PS-1 results in increased PS-1/GSK3β association and increased phosphorylation of tau (22). Furthermore, PS-1 forms a complex with the GSK3β substrate β-catenin in transfected cells (23, 24) and *in vivo* (23, 25), and this interaction increases β-catenin stability (25). Pathogenic PS-1 mutations reduce the ability of PS-1 to stabilize β-catenin, which in turn results in decreased β-catenin levels in brains from AD patients with PS-1 mutations (25). GSK3β phosphorylates pyruvate dehydrogenase and inhibits it in response to β-amyloid; as a consequence, a reduction in ATP and ACh synthesis has been described in hippocampal neurons (26). Taken together, these data indicate that GSK3β is located at the convergence of pathways involved in AD-like tau hyperphosphorylation, β-amyloid-induced toxicity, PS-1 mutations, and ACh metabolism, all of which are relevant to AD. Recent evidence using lithium and short interfering RNAs directed toward GSK3α block the production of Aβ by interfering with APP at the γ-secretase step but not Notch processing (51). The effects of the GSK3 inhibitor lithium was observed in cells, as well as in transgenic mice that overproduce APP.

An increase in GSK3 levels or activity in AD post mortem tissue, compared with non-diseased human brain, has been described by several researchers. Using active site antibodies, GSK3 has been shown to localize to pretangle neurons, dystrophic neurites, and NFTs in AD brain (12). Neurons actively undergoing granulovacular degeneration are also immunopositive for active GSK3 (27). A spatial and temporal pattern of increased active GSK3β expression coinciding with the progression of NFT and neurodegeneration has been reported (11). Taken together, these studies provide evidence that the active form of GSK3β is increased in AD brain. Because active GSK3β triggers signal transduction events that participate in cell death (28, 29), and loss of neuronal and synaptic plasticity (30), a significant part of the AD pathology could result from an abnormal increase in GSK3β expression and activity.

When GSK3β transgene expression is induced in brain, adult mice developed hyperphosphorylated tau at the PHF-1 site (phospho-epitope at Ser-396/404) (31), a site critical for PHF formation and represents increased phosphorylation in AD brain (32). These mice also developed pretangle structures in the hippocampus, as well as increased neuronal death, gliosis, and spatial learning deficits in the Morris water maze (33). Overexpression of human tau, in combination with its phosphorylation by the *Drosophila* GSK3β homologue Shaggy, exacerbates neurodegeneration induced by tau overexpression alone and gives rise to NFT pathology in the fly (34). Taken together, these studies provide strong evidence that increased GSK3β expression and activity are necessary for the early events leading to pretangle and neurodegenerative pathology that is associated with AD.

Accordingly, several groups have identified small molecule GSK3 inhibitors (35–40). However, the majority of the reported inhibitors are not selective against GSK3 and also affect cdk2, a kinase that shares 33% amino acid identity with GSK3, or cdk5, another protein kinase involved in tau phosphorylation. In addition, there is a lack of basic information about the structural basis of the interaction between GSK3β and these inhibitors, as co-crystallization studies have not been reported. Here, we report the identification and characterization of a thiazole, *N*-(4-methoxybenzyl)-*N*′-(5-nitro-1,3-thiazol-2-yl)urea (AR-A014418), which is a selective and potent inhibitor of GSK3 able to decrease tau phosphorylation and cell death. Furthermore, the co-crystallization of AR-A014418 with the GSK3β protein provides the structural information required to understand the high selectivities of this inhibitor.

EXPERIMENTAL PROCEDURES

Materials

Propidium iodide (PI) was purchased from Sigma and calcein-AM from Molecular Probes. Antibody Tau5 was purchased from Research Diagnostics Inc., and tau Ser(P)-396 was from BIOSOURCE International. Anti-GSK3β was from Transduction Laboratories. The peptide β-amyloid 25–35 was from Bachem and was prepared as described previously (48, 49). The biotinylated eukaryotic initiation factor 2B (eIF2B) peptide, biotin-AAEELDSRAGS(PO_3H_2)PQL, was synthesized at AstraZeneca R&D Lund (Lund, Sweden). A peptide based on glycogen synthase, RRRPASVPPSPSLSRHS-S(PO_4)-HQRR, was produced by Auspep Pty. Ltd. (Parkville, Australia). The biotinylated peptide biotin-AKKPKTPKKAKKL-OH used in cdk5 assay was produced by Bachem AG (Bubendorf, Switzerland). Glutathione *S*-transferase (GST)-retinoblastoma expressed in a GST expression system and cdk5/p25 (co-transfected 2:5) were supplied by AstraZeneca Biotech Laboratory (Södertälje, Sweden). Recombinant human GSK3 was obtained from Dundee University (Dundee, Scotland, United Kingdom) and contained a mixture of GSK3β and GSK3α to a minor extent. Baculoviral cdk2/cyclin E enzyme was supplied by Enabling Science & Technology Biology Department, AstraZeneca R&D, Alderley Park, United Kingdom. [γ-^{33}P]ATP, protein A, and streptavidin-coated scintillation proximity assay (SPA) beads were purchased from Amersham Biosciences UK.

Chemistry

The synthesis of AR-A014418 is outlined in Scheme I.

In brief, commercially available 2-amino-5-nitrothiazole and 4-methoxybenzylisocyanate was mixed in *N*,*N*-dimethylformamide to give AR-A014418 in 22% yield. The aqueous solubility of AR-A014418 was determined to be 136 μM.

N-(4-Methoxybenzyl)-N′-(5-nitro-1,3-thiazol-2-yl)urea Synthetic Procedure

A mixture of 2-amino-5-nitrothiazole (0.89 g, 6.13 mmol) and 4-methoxybenzylisocyanate (1 g, 6.13 mmol) in *N*,*N*-dimethylformamide (6 ml) was heated at 100 °C under nitrogen atmosphere for 15 h. The mixture was allowed to cool and was partitioned between water and ethyl acetate. The aqueous layer was extracted with another portion of ethyl acetate. The combined organic layers were washed with brine, dried ($MgSO_4$), and evaporated to give 2.5 g of a semisolid crude product. Most of the material was dissolved in chloroform/ethanol (98:2, approximately 15 ml) and triethylamine (3 ml), followed by filtration. The dissolved crude product was purified on a silica gel column using chloroform/ethanol (95:5) as the eluent to give 408 mg (22% yield) of the title compound as a yellowish solid: mp >190 °C (decomposition); ^{1}H NMR (Me_2SO-d_6, 400 MHz) δ 11.64 (br s, 1 H), 8.50 (s, 1 H), 7.25–7.23 (m, 3 H), 6.92–6.89 (m, 2 H), 4.30 (d, J = 5.9 Hz, 2 H), 3.73 (s, 3 H); ^{13}C NMR (Me_2SO-d_6, 100 MHz) δ 164.42, 158.43, 153.48, 143.47, 140.80, 130.82, 128.72, 113.82, 55.08, 42.60; MS(ES) m/z 309 (M^+ + 1).

Protein Purification and Expression of Material Used for Crystallization

Full-length human GSK3β was cloned into the NdeI and EcoRI restriction sites of pET28a(+) (Novagen) via the PCR Script vector

(Stratagene) using the PCR primers 5′-CATCATATGTCAGGGCGGC-CCAGAACC and 5′-TCATCAGGTGGAGTTGGAAGCTGATGC.

An NcoI-EcoRI gene fragment was subsequently subcloned into pFASTBAC HTb (Invitrogen) resulting in a construct with an N-terminal double histidine tag with the following amino acid sequence: MSYY-HHHHHHDYDIPTTENLYFQGAMGSSHHHHHHSSGLVPRGSH-. Briefly, Sf21 cells were transfected with recombinant bacmid DNA using Superfect (Qiagen) and incubated for 3 days at 27 °C. The virus particles were amplified in Sf21 cells for 7 days and titrated using the Clontech titration kit.

High Five cells were grown at 27 °C in a 20-liter cell culture bioreactor (BBI) in Expression High Five SFM medium (Invitrogen), supplemented with 12 mM L-glutamine, 5 mM asparagine, and 0.1% NaCl. The culture was infected with the recombinant baculovirus with a multiplicity of infection of 2 at a cell density of 2.12×10^6 cells/ml. The cells were harvested 46 h after infection using a Contifug Stratos centrifuge. The cells were washed with PBS, frozen, and stored in −80 °C prior to purification. The cells were thawed, resuspended in lysis buffer (20 mM HEPES, pH 7.0, 500 mM NaCl, 10 mM imidazole, 10% (v/v) glycerol, 1 mM Tris (2-carboxyethyl) phosphine, and EDTA-free Complete Protease Inhibitor, Roche Diagnostics) to a density of 20×10^6 cells/ml, and then lysed by using an Ultra-Turrax T50 (Janke & Kunkel). The cell debris was removed by centrifugation for 30 min at 3 °C and $35{,}000 \times g$ using an Avanti J-20 with a JLA 16.250 rotor (Beckman). Chelating Sepharose Fast Flow (Amersham Biosciences), previously loaded with 0.5 bed volume of 0.1 M Ni_2SO_4, was added in a ratio of 2 ml of Sepharose/10^9 cells, and GSK3β was allowed to adsorb to the matrix in a batch fashion for 60 min at 4 °C. All subsequent steps were performed at room temperature. Unbound protein was removed with Buffer A (lysis buffer without protease inhibitor) using a sintered glass filter funnel, and the resin was packed into a column, further washed with Buffer A, and then washed with Buffer A containing 250 mM imidazole. GSK3β protein was finally eluted with Buffer A containing 500 mM imidazole. GSK3β-containing fractions were pooled and loaded onto a Sephadex G25 column equilibrated with Buffer B (20 mM HEPES, pH 7.0, 350 mM NaCl, 5% (v/v) glycerol, and 1 mM Tris (2-carboxyethyl) phosphine. The final protein was aliquoted, frozen, and stored in −80 °C. Approximately 8 mg of >95% pure GSK3β was produced per liter of cultivation.

The histidine tag was removed by thrombin cleavage using 500 units of thrombin (Amersham Biosciences)/70 mg of protein for 4 h at room temperature and cleavage at a second site (after arginine 6) was observed. A residual thrombin activity remained despite later purification steps, and the protein preparation used for crystallization was a mix of full length and the 7–420 species. Unphosphorylated and phosphorylated GSK3β was separated using a 6-ml Resource S column (Amersham Biosciences), equilibrated in 20 mM HEPES, pH 7.0, 80 mM NaCl, 2 mM DTT, and 5% glycerol, using a 20-column volume gradient from 80 to 350 mM NaCl. Full-length unphosphorylated GSK3β eluted at approximately 200 mM NaCl, and the peak fractions were pooled and concentrated to 6.3 mg/ml (λ_{280} = 34,960 M^{-1} cm^{-1}).

Crystallization

Crystals were grown using the hanging drop method. A 1.5 + 1.5-μl drop consisting of protein solution (130 μM GSK3β, 250 μM AR-A014418, 20 mM HEPES, pH 7.0, 200 mM NaCl, 2 mM DTT, 5% glycerol, and 1.3% Me_2SO) and well solution (17% polyethylene glycol 3350, 50 mM BisTris propane, pH 6.5, and 5 mM urea) was placed over 500 μl of well solution at 20 °C. Crystals grew within a few days to a size of 100 μm and were soaked in cryo solution (15% glycerol, 10% polyethylene glycol 3350, 100 mM NaCl, and 50 mM BisTris propane, pH 6.5) before being frozen in a 100 K nitrogen stream.

Data Collection and Structure Determination

All the structure descriptions in this paper are based on the refined structure using the synchrotron data. Details of data collection and refinement statistics are recorded in Table I. The current R-factor/R_{free} is 0.22/0.24. Data were first collected using in-house x-ray source (CuK_α radiation; wavelength = 1.54 Å) to a resolution of 3.1 Å on a MarResearch 345-mm image-plate detector system. X-ray radiation was generated by a Rigaku RU300HB rotating anode operated at 50 kV and 100 mA. The crystal belongs to orthorhombic space group $P2_12_12_1$, with cell parameters of a = 82.028 Å, b = 84.215 Å, and c = 178.091 Å. Molecular replacement was carried out with program MOLREP using overlaid structures of cdk2, ERK, and p38g as the search model. To prepare the search model, these three structures were first superimposed using program MAPS, and then each was trimmed manually in the program O to remove some loop regions to ~260 residues, respectively. MOLREP found two molecules after rotation and translation search with R-factor/correlation coefficient of 0.514/0.280. Phase improvement with solvent flattening (solvent content 0.622) and 2-fold density averaging was performed using the program DM. The solution was verified by inspection of the calculated electron density map in program O after phase improvement. Subsequently the cdk2 model from molecular replacement was used for initial refinement and model building. A high resolution data set (1.94 Å) was later collected at beamline ID29 (wavelength of 1.0064 Å) in ESRF (Grenoble, France).

Kinase Assays

GSK3 Scintillation Proximity Assay—The competition experiments were carried out in duplicate with 10 concentrations of the inhibitor in clear-bottomed microtiter plates. The biotinylated peptide substrate, biotin-AAEELDSRAGS(PO_3H_2)PQL, was added at a final concentration of 2 μM in an assay buffer containing 6 milliunits of recombinant human GSK3 (equal mix of both α and β), 12 mM MOPS, pH 7.0, 0.3 mM EDTA, 0.01% β-mercaptoethanol, 0.004% Brij 35, 0.5% glycerol, and 0.5 μg of bovine serum albumin/25 μl and preincubated for 10–15 min. The reaction was initiated by the addition of 0.04 μCi of [γ-^{33}P]ATP and unlabeled ATP in 50 mM $Mg(Ac)_2$ to a final concentration of 1 μM ATP and assay volume of 25 μl. Blank controls without peptide substrate were used. After incubation for 20 min at room temperature, each reaction was terminated by the addition of 25 μl of stop solution containing 5 mM EDTA, 50 μM ATP, 0.1% Triton X-100, and 0.25 mg of streptavidin-coated SPA beads corresponding to ~35 pmol of binding capacity. After 6 h the radioactivity was determined in a liquid scintillation counter (1450 MicroBeta Trilux, Wallac).

cdk2 Scintillation Proximity Assay—The competition experiments were carried out in duplicate with 10 concentrations of the inhibitor in clear-bottomed microtiter plates. cdk2/cyclin E enzyme was added at a concentration corresponding to a 80× dilution of the partially purified baculovirus-infected insect cell lysate in a buffer containing 50 mM HEPES, 10 mM $MnCl_2$, 1 mM DTT, 100 μM NaF, 100 μM sodium O-vanadate, 10 mM sodium glycerophosphate, 5 μg/ml aprotinin, 2.5 μg/ml leupeptin, and 100 μM phenylmethylsulfonyl fluoride. Blank controls without enzyme were used. The reaction was initiated by the addition of 1.25 μg of GST-retinoblastoma (part of the retinoblastoma gene (792–928) expressed in a GST expression system and purified from *E. coli*), 0.15 μCi of [γ-^{33}P]ATP, and unlabeled ATP at a final concentration of 0.1 μM; the final assay volume was 50 μl. After incubation for 60 min at room temperature, each reaction was terminated by the addition of 150 μl of stop solution containing 45 μl of protein A-coated SPA beads in 50 mM HEPES, 3.28 μg of anti-glutathione S-transferase, 5.5 mM EDTA, and 35 μM ATP. The plate was centrifuged at 2000 rpm for 5 min and the radioactivity determined as previously described.

cdk5 Scintillation Proximity Assay—cdk5/p25 enzyme was diluted to give a final concentration of 0.2 ng/μl (3.3 nM) in enzyme buffer containing 70 mM HEPES, 0.5 mM EDTA, 37.5 mM KCl, 30 mM β-glycerophosphate, 0.15% bovine serum albumin (w/v), 0.05% β-mercaptoethanol (v/v), 0.02% Brij 35 (w/v), and 2.55 glycerol, pH 7.35. The competition experiments were carried out in duplicate with 10 concentrations of the inhibitor in clear-bottomed microtiter plate. cdk5/p25 enzyme was added followed by a short centrifugation (~700 rpm for 10 s) and 15-min preincubation. Blank controls without enzyme were used. The reaction was initiated by addition of biotinylated peptide (bio-AKKPKTPKKAKKL-OH) to a final concentration of 5 ng/μl (2.95 μM) together with 0.07 μCi of [γ-^{33}P]ATP solution, giving a final concentration of 2 μM ATP followed by a short centrifugation and incubation for 40 min. The final assay volume was 21 μl. The reaction was terminated by adding 30 μl of stop solution containing 40 mM EDTA, 3.7 mM ATP, and 7.5 mg/ml SPA beads corresponding to ~30-pmol binding capacity. The plate was centrifuged at 2000 rpm for 2 min and the radioactivity determined as previously described.

Kinetic Studies—For the determination of inhibition mechanisms, the activity of GSK3β was determined in duplicate for all combinations between ATP concentrations 7.81, 15.6, 31.3, 62.5, 125, and 250 μM (K_m ~ 20 μM) and inhibitor concentrations of 0, 49.4, 148, 444, 1330, and 4000 nM. The concentration of GSK3β was 0.02 unit/ml (~1 nM), and the concentration of the GS-peptide substrate (RRRPASVPPSPSLSRHS-S(PO_4)-HQRR) was 20 μM. The reactions were started with ATP solutions containing 110 Ci of [γ-^{33}P]ATP/mol of ATP. The reaction was run for 15 min in room temperature and then stopped by addition of an excess of EDTA and "cold" ATP. 10 μl of the samples were spotted on a P30 filter (PerkinElmer Life Sciences, Finland) and washed four times for 5 min each in 75 mM phosphoric acid. The filter was dried, treated with Meltilex melt-on scintillator (PerkinElmer Life Sciences), and

counted in Trilux Microbeta scintillation counter (PerkinElmer Life Sciences).

IC_{50} Determination

Inhibition curves were analyzed by non-linear regression using GraphPad Prism (GraphPad Software, Inc., San Diego, CA). The inhibition constants (K_i) of the test compound were calculated from observed IC_{50} of the test compound using the equation of Cheng and Prusoff (50). The K_m value of ATP used to calculate the inhibition constants (K_i) of the various compounds was 20 μM for GSK3β, 0.5 μM for cdk2, and 10 μM for cdk5.

The activity of AR-A014418 against 26 kinases was studied as described (41) using an ATP concentration of 100 μM (data obtained in collaboration with P. Cohen, University of Dundee, Dundee, Scotland, United Kingdom).

Analysis of Tau Phosphorylation

3T3 fibroblasts were engineered to stably express four-repeat tau protein. These cells have high endogenous levels of GSK3 that is able to phosphorylate tau protein constitutively. This phosphorylation is inhibited by LiCl. After treatment with different compounds, cultures were washed twice with 5 mM $MgCl_2$-PBS. Extracts for Western blot analysis were prepared by homogenizing cells in ice-cold extraction buffer consisting of 20 mM HEPES, pH 7.4, 100 mM NaCl, 10 mM NaF, 1% Triton X-100, 1 mM sodium orthovanadate, 10 mM EDTA, and protease inhibitors (2 mM phenylmethylsulfonyl fluoride, 10 μg/ml aprotinin, 10 μg/ml leupeptin, and 10 μg/ml pepstatin). The samples were homogenized at 4 °C, and protein content was determined by Bradford method. Total protein (25 μg) was electrophoresed on 10% SDS-PAGE gel and transferred to a nitrocellulose membrane (Schleicher & Schuell). The experiments were performed using the following primary antibodies: tau Ser(P)-396, 1:1000; Tau5, 1:1000; and anti-GSK3β, 1:1000. The filters were incubated with the antibody at 4 °C overnight in 5% nonfat dried milk. A secondary horseradish peroxidase-linked sheep anti-mouse (Tau5, GSK3β, Amersham Biosciences) or horseradish peroxidase-linked donkey anti-rabbit (tau Ser(P)-396) antibody (both 1:5000; Amersham Biosciences), followed by ECL detection reagents (Amersham Biosciences), were used for immunodetection. Quantitation of immunoreactivity was performed by densitometric scanning.

Cell Viability Assays

Cell viability was assessed by calcein/propidium iodide uptake (42). Calcein AM is taken up and cleaved by esterases present within living cells, yielding yellowish-green fluorescence, whereas PI is only taken up by dead cells, which become orange-red fluorescent. In brief, N2A cells were cultured for 2 days *in vitro* and then treated with 50 μM LY-294002 in the presence of AR-A014418 or vehicle (Me_2SO) for 24 h. Subsequently, N2A cells were incubated for 30 min with 2 μM PI and 1 μM calcein-AM. The cultures were then rinsed three times with Hanks' buffered saline solution containing 2 mM $CaCl_2$, and the cells were visualized by fluorescence microscopy using a Zeiss Axiovert 135 microscope. Three fields (selected at random) were analyzed per well (~300 cells/field) in at least three different experiments. Cell death was expressed as percentage of PI-positive cells from the total number of cells. In every experiment, specific cell death was obtained after subtracting the number of dead cells present in vehicle-treated cultures.

Neurodegeneration Mediated by β-Amyloid Peptide: Organotypic Cultures

Organotypic cultures were prepared essentially according to Studer *et al.* (48), with modifications described by Luthman *et al.* (49). Three-day postnatal Sprague-Dawley rat pups were sacrificed by decapitation and their brains removed under sterile conditions. The hippocampus was dissected out, placed in Gray's balanced salt solution (Life Technologies, Inc.), and thereafter cut into 250-μm-thick slices with a tissue chopper (McIllwain). The slices were transferred to a Petri dish containing 2 ml of Gray's balanced salt solution. The tissue pieces were then placed on 12 × 24-mm glass cover slips, embedded by means of two drops of reconstituted chicken plasma (Sigma), and coagulated by one drop of thrombin solution (Sigma). After coagulation in 30 min at room temperature, the cover slips were transferred into sterile plastic tubes containing 1.1 ml of medium. The medium consisted of 55.0 ml of Dulbecco's modified Eagle's medium with glutamine (Life Technologies, Inc.), 32.5 ml of Hank's balanced salt solution, 1.5 ml of a 20% glucose solution (Life Technologies, Inc.), and 1.0 ml of HEPES solution (2.39 g of HEPES; WWR in 10 ml of distilled water tissue culture tested; Life Technologies, Inc.); 10 ml of heat-inactivated fetal calf serum 1% antibiotic-antimycotic solution (Life Technologies, Inc.) was also added. The tubes were transferred to an incubator and placed in a roller drum (Bellco), tilted at an angle of 5° to the horizontal axis, which rotated at 60 revolutions/h. The incubation was performed at 37 °C at a humidity of ~95–98%, and with a CO_2 concentration of 5%. Fresh medium was prepared every week without antibiotic-antimycotic solution added.

After 21 days *in vitro*, amyloid-β peptide (25–35) (Aβ) dissolved in distilled water was added to the medium at a final concentration of 50 μM. Control cultures were grown in parallel with the cultures which were exposed to Aβ, with fresh medium changed every other day. AR-A014418 at concentrations of 3, 10, or 30 μM was added at the same time as Aβ AR-A 014418 at a concentration of 30 μM was also studied without any addition of Aβ. Stock solutions of those compounds were prepared in Me_2SO with a final Me_2SO concentration of 0.01%. The medium was changed once (day 2) during the 4-day Aβ exposure. Fresh solutions were made each time.

Histology

Following 4 days of Aβ exposure, the cultures were fixed for 30 min at room temperature in 0.4% formaldehyde and 0.125% glutaraldehyde in 0.1 M phosphate-buffered saline (PBS; pH 7.4). After rinsing three times in 0.1 M PBS, the cultures were incubated with a mouse monoclonal primary antibody raised against the NMDA-R1 subunit of the NMDA receptor (diluted 1:600) for 3 days at 4 °C in 0.1 M PBS containing 0.3% Triton X-100 and 1.5% normal horse serum. The cultures were thereafter washed in PBS, and incubated with biotinylated secondary antiserum for 30 min in PBS/Triton X-100 buffer including 1.5% normal horse serum. The cultures were subsequently washed three times in PBS, and then incubated in PBS/Triton X-100 buffer for 1 h to obtain the avidin-biotin complex (ABC-Elite kit; Vectastain). The cultures were thereafter washed twice, first in PBS for 10 min and then in 50 mM Tris-HCl buffer, pH 7.4. Chromogen reaction was performed by incubation in 0.1 M Tris-HCl buffer containing diaminobenzidine tetrahydrochloride, at a concentration of 1 mg/ml, and 0.2% H_2O_2. The diaminobenzidine tetrahydrochloride reaction was terminated by washing the cultures in PBS. After dehydration in a graded series of ethanol, followed by xylene, the cultures were mounted on glass slides using Eukitt. The number of NMDA-R1 immunoreactive cells, which showed processes and pyramidal shape, were counted in each culture using light microscopy (magnification, ×10).

RESULTS

AR-A014418 Inhibits GSK3 in Vitro

The chemical structure of the thiazole AR-A014418 is shown in Fig. 1*A*. AR-A014418 inhibits recombinant human GSK3 with an IC_{50} value of 104 ± 27 nM (Fig. 1*B*). The IC_{50} was determined using a scintillation proximity assay with a biotinylated peptide sequence from one eIF2B and [γ-^{33}P]ATP as substrates. Cdk2 is the nearest kinase from a homology perspective (overall 33% amino acid identity), and almost all of the reported GSK3 inhibitors also inhibit other cdks such as cdk2 or cdk5 (see above). Therefore, the effect of AR-A014418 was determined on these kinases. AR-A014418 did not significantly inhibit either cdk2/cyclin E or cdk5 (K_i > 100 μM; Fig. 1*B*), demonstrating the specificity of AR-A014418 with respect to GSK3. AR-A014418 (10 μM) did not significantly inhibit any kinase (26 kinases) tested in a pan-kinase screen performed at the University of Dundee (Fig. 1*C*).

Kinetic analyses were performed using combinations of six ATP concentrations up to 200 μM (K_m ~ 20 μM) and six inhibitor concentrations from 0 to 40 times the IC_{50} of the inhibitor, *i.e.* up to 4 μM. AR-A014418 shows an inhibition mechanism consistent with ATP competition and a K_i value of 38 nM, as shown by nonlinear regression analysis (Fig. 1*D*) and illustrated in the Lineweaver-Burke plot in Fig. 1*E*.

Co-crystallization of GSK3β with AR-A014418

The data collection, refinement, and model assessment statistics of the crystal structure are shown in Table I. The refined model contains two GSK3β molecules, each with a bound inhibitor, in total 689 amino acid residues (5521 protein atoms),

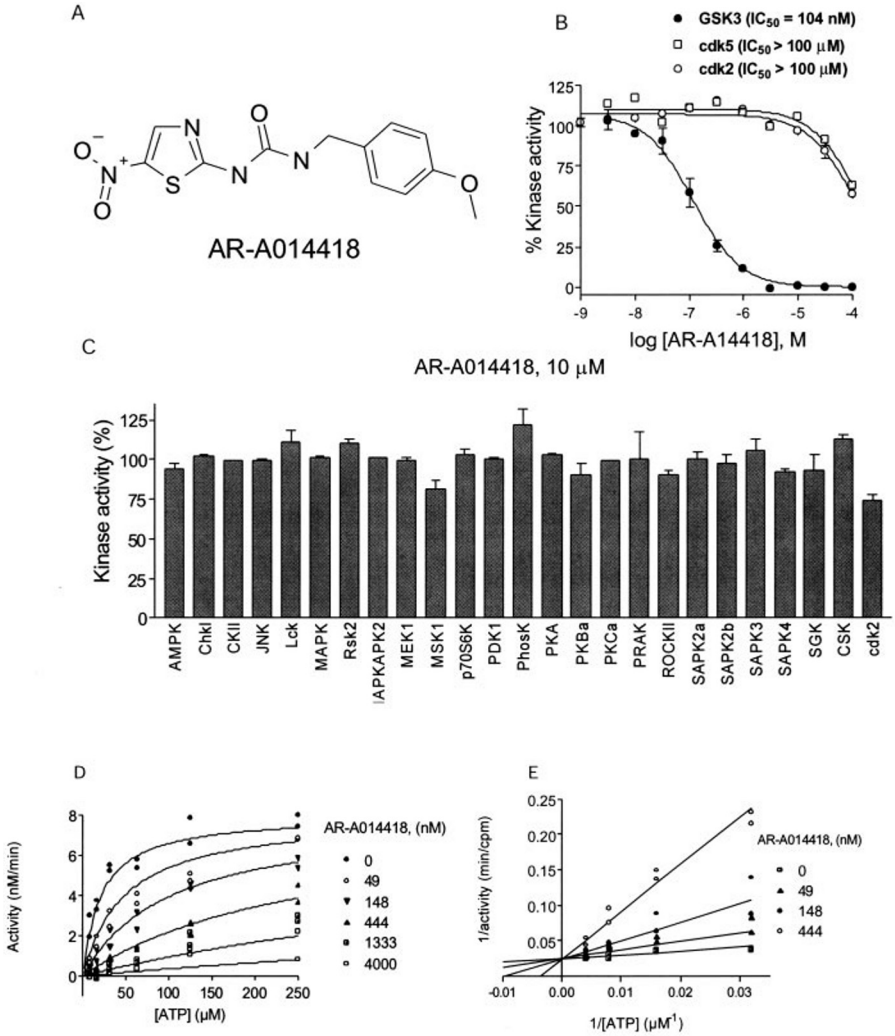

FIG. 1. **AR-A014418 specifically inhibits GSK3*β*.** *A*, the chemical structure of AR-A014418; *B*, AR-A014418 inhibits GSK3β activity *in vitro*. The ability of recombinant human GSK3β (●) to phosphorylate eIF2B substrate was assayed in the presence of the indicated concentrations of AR-A014418 (IC_{50} = 104 ± 27 nM). The ability of AR-A014418 to inhibit cdk5 (□) and cdk2 (○) was also analyzed (IC_{50} >100 μM). Results are presented as the percentage of the respective kinase activity in the absence of the compound. Data are mean ± S.E. from three independent experiments performed in duplicate. *C*, effect of AR-A014418 on the activities of 26 protein kinases *in vitro*. Protein kinases were assayed in the presence of 10 μM AR-A014418 or vehicle (*DMSO*). The enzymatic activity was carried out in the presence of 0.1 mM ATP. Kinase activities are given as the mean of triplicate determinations. *AMPK*, AMP-activated protein kinase; *Chk*, checkpoint kinase; *CKII*, casein kinase-2; *JNK*, c-Jun N-terminal kinase; *Lck*, lymphocyte c-Src kinase; *MAPK*, mitogen-activated protein kinase; *Rsk2*, ribosomal S6 kinase-2; *MAPKAPK-2*, mitogen-activated protein kinase-activated protein kinase-2; *MEK1*, mitogen-activated protein kinase/extracellular signal-regulated kinase kinase-1; *MSK1*, mitogen- and stress-activated protein kinase-1; *p70 S6K*, p70 ribosomal protein S6 kinase; *PDK1*, 3-phosphoinositide-dependent protein kinase-1; *PhosK*, phosphorylase kinase; *PKA*, protein kinase A; *PKBa*, protein kinase B; *PKCa*, protein kinase C; *PRAC*, p38-regulated/activated kinase; *ROCKII*, Rho-dependent protein kinase II; *SAPK*, stress-activated protein kinase; *SGK*, serum- and glucocorticoid-induced kinase; *CSK*, carboxyl-terminal Src kinase; *cdk2*, cyclin-dependent kinase 2. *D* and *E*, kinetic studies. *D*, GSK3 inhibition determined by increasing concentrations of AR-A014418 in the presence of different ATP concentrations. The *lines* represent the result of a non-linear regression analysis of the entire data set using a kinetic model for mixed inhibition. The analysis showed a competitive inhibition with ATP and a K_i of 38 nM. *E*, double-reciprocal plots of GSK3 activity in the presence of varying concentrations of ATP and AR-A014418. Excerpt of data from *D* selected for clarity. The *lines* are linearized versions of the result of the non-linear regression analysis in *D*. *Lines* intersecting on the *y* axis indicate competitive inhibition with respect to ATP.

two bound inhibitor (42 atoms), and 373 water molecules. The current *R*-factor/R_{free} is 0.22/0.24. Root mean square deviation from ideal values for bond lengths and bond angles are 0.006 Å and 1.2°, respectively. The overall quality of the current refined structure is good, as judged by the electron density map, refinement statistics, and output from PROCHECK (52). The estimated coordinate error is 0.26 and 0. 21 Å, based on the Luzzati plot and the SigmaA method, respectively. More statistics are compiled in Table I. The electron density map calculated from the currently refined model shows good quality (see Fig. 2), except some surface loop regions that are far (more than ~15 Å) from the ATP site.

The crystal structure of GSK3β bound to AR-A014418 reveals the interactions formed and provides an explanation for the specificity of the compound on GSK3β. The structure has the typical kinase conformation of the activated form, although the actual protein used for this study is not phosphorylated at Tyr-216. This was later confirmed by the structure of the phosphorylated GSK3β in complex with the peptide FRATide, peptide inhibitor of GSK3 (data not shown). The main difference is the rotamer conformation of Tyr-216, which appears to have rotated 180°. However, the main chain trace of the phosphorylation loop basically remains unchanged (Fig. 3, *A* and *B*). Comparison of the two molecules in the dimer showed very small difference between them. Superposition by least square fitting yielded a root mean square distance of 0.39 Å of the 314 α-carbon atoms.

TABLE I
Crystallography: data collection and refinement statistics

Data collection	In-house data (λ = 1.54 Å)	Synchrotron data, ID29 European Synchotron Radiation Facility (λ = 1.0064 Å)
Space group	$P2_12_12_1$	$P2_12_12_1$
Cell parameter (Å)	82.03, 84.21, 178.09	82.58, 84.91, 178.42
Solvent content (%)	62.9	63.5
Resolution (last shell) (Å)	3.11 (3.11-3.30)	1.94 (1.94-2.04)
Unique reflections	21,482	78,815
R_{merge} (all/last shell)	0.290/0.669	0.071/0.431
I/I_s (all/last shell)	2.4/1.1	7.1/1.7
Completeness (%) (all/last shell)	94.3/93.4	84.4/58.9
Redundancy	3.7	7.2
Structure refinement		
Resolution (last shell) (Å)		1.94 (1.94-2.06)
Number of reflections used (last shell)		78,753 (9134)
Fraction of test set for calculating R_{free} (%)		3.4
No. of reflections in the test set (last shell)		2670 (310)
R_{work} (last shell)		0.222 (0.274)
R_{free} (last shell)		0.243 (0.291)
Root mean square deviation bond lengths (Å)/bond angles (°)		0.006/1.2
Estimated coordinate error (Luzzati plot/ SigmaA) (Å)		0.26/0.21
B values (mean *B* value/Wilson plot) (Å^2)		40.4/41.3
Number of atoms: final model (protein/waters/ligand)		5521/373/42

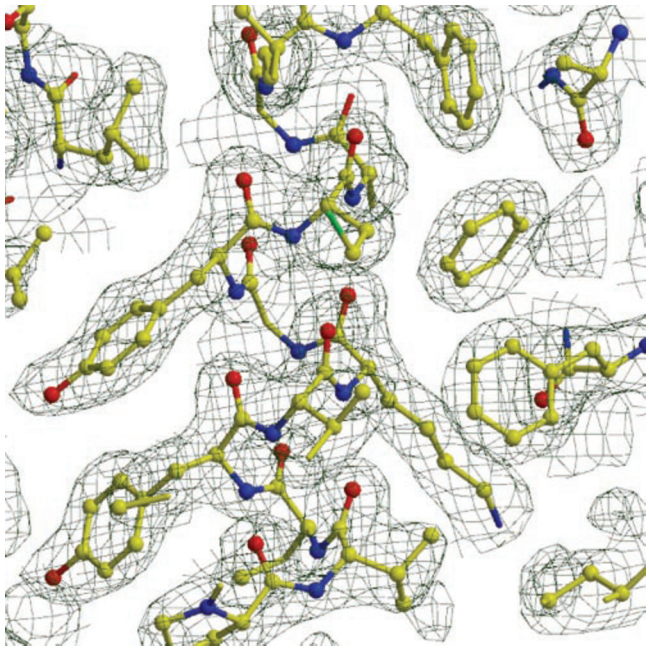

FIG. 2. **Electron density map showing part of an alpha helix in the structure.** Figure shows a $2F_o - F_c$ map, calculated from the currently refined model, contoured at 1.0 σ.

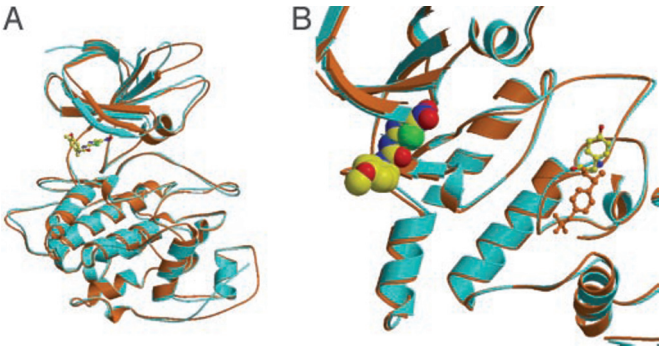

FIG. 3. **Ribbon diagram of the GSK3β in complex with AR-A014418.** *A*, overlay of the GSK3β unphosphorylated (in *cyan*) and phosphorylated (in *orange*) form. *B*, magnification of the substrate binding groove. The superposition of both GSK3β forms shows that, when Tyr-216 is phosphorylated, this allows the substrate to bind to the substrate groove. The AR-A014418 is represented as space-filling atoms.

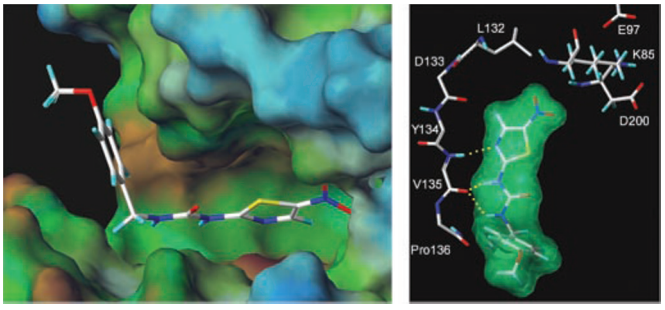

FIG. 4. **Binding of AR-A014418 to GSK3β.** *Left*, surface representation of the inhibitor binding pocket. *Right*, interactions between the ligand and the protein. For clarity only residues in the linker/hinge region and those involved in the important ion-pair interaction (Lys-85, Glu-97, and Asp-200) are shown. Hydrogen bonds between the inhibitor and the protein molecule are shown as *yellow lines*. *Single-letter codes* are used for amino acids.

Structure of AR-A014418 Bound to GSK3b

Co-crystals of AR-A014418 and GSK3β reveal AR-A014418 bound within the ATP pocket (Fig. 4*A*). AR-A014418 binds along the hinge/linker region of the GSK3β having three hydrogen bond interactions to the main chain atoms of the protein (Fig. 4*B*). The nitro group of the inhibitor occupies the inner part of the ATP pocket; the closest distance between the nitro O to the selectivity residue Leu-132 is only 3.03 Å. The other end group from the inhibitor, the phenyl ring, takes an orientation that is ~108° out of the plane of the core inhibitor, such that it fits in stacking interaction to the guanidine group of Arg-141 (3.8 Å).

Biological Effects of AR-A014418

Tau Phosphorylation—To evaluate whether AR-A014418 inhibits GSK3β-mediated tau phosphorylation in cells, 3T3 fibroblasts were engineered to stably express four-repeat tau protein. Transfected cells were treated with vehicle (0.1% Me_2SO) or with increasing concentrations (100 nM to 50 μM) of AR-A014418 and harvested at 4 h after treatment. The effect on tau phosphorylation in the presence and absence of serum was determined by Western blotting. Detection was carried out

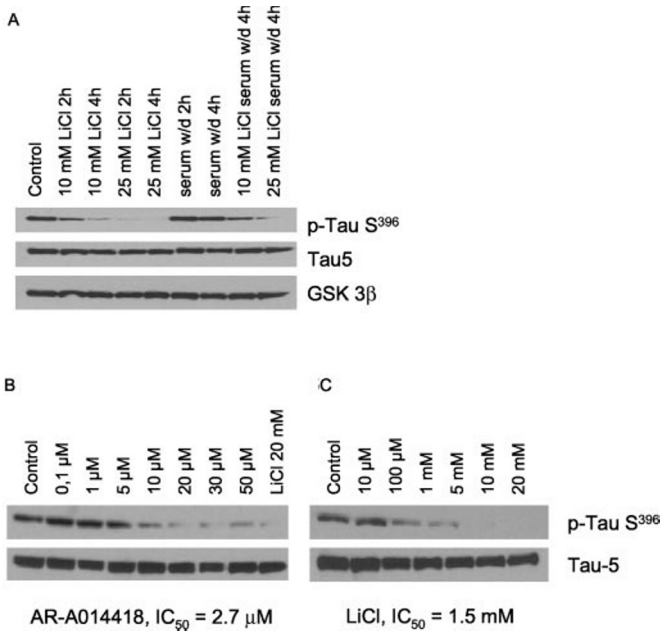

FIG. 5. **AR-A014418 inhibits tau phosphorylation in cells.** 3T3 fibroblasts were engineered to stably express four-repeat tau protein. *A*, cells were treated with 10 and 25 mM lithium for 2 and 4 h in the presence or absence of serum. The effect on tau phosphorylation was determined by Western blotting, and detection was carried out using a phosphospecific antibody on tau (*p-Tau S*^{396}). Total levels of tau in the samples were determined by stripping the blot and reprobing it with a phosphorylation-independent antibody to total tau protein (*Tau5*). The bands were quantified by densitometric analysis. Lithium inhibited tau phosphorylation in the presence or absence of serum. Total levels of tau and GSK3 were similar between samples. *B*, cells were treated with vehicle (0.1% Me_2SO) or increasing concentrations (100 nM to 50 μM) of AR-A014418 and harvested at 4 h after treatment. AR-A014418 inhibited tau phosphorylation in cells in a dose-dependent fashion, exhibiting an IC_{50} of 2.5 μM. *C*, effects were compared with lithium chloride, a reference GSK3β inhibitor (IC_{50} = 1.5 mM).

using a phosphospecific antibody, which detects an epitope on tau (Ser(P)-396), a site specifically phosphorylated by GSK3 in cells. Total levels of tau in the samples were determined by stripping the blot and reprobing it with a phosphorylation independent antibody to total tau protein (Tau5). The bands were quantified by densitometric analysis. The levels of Ser(P)-396 were not affected by changes in serum, and lithium was effective at inhibiting tau phosphorylation under both conditions (Fig. 5*A*). AR-A014418 inhibits tau phosphorylation in the transfected cells in a dose-dependent fashion exhibiting an IC_{50} of 2.7 μM, as shown in Fig. 5*B*. AR-A014418 effects were compared with lithium chloride (IC_{50} = 1.5 mM), a reference GSK3β inhibitor (43). AR-A014418 was a more potent inhibitor of GSK3β than lithium (Fig. 5, *B* and *C*). A similar IC_{50} was obtained for the inhibition of okadaic acid-induced hyperphosphorylation of endogenous tau in SY5Y human neuroblastoma cells (data not shown).

Neuronal Death—Previous studies have demonstrated that GSK3β is phosphorylated on Ser-9 and inhibited by the PI3K/PKB survival pathway, which normally suppresses apoptosis (28, 29). To evaluate the effects of AR-A014418 on neuroprotection, LY294002, a PI3K inhibitor (44), was used. This treatment inactivates the PI3K/PKB survival pathway, thereby activating GSK3β. We show that AR-A014418 protects neuroblastoma N2A cells in culture from death induced by reduced PI3K pathway activity in a dose-dependent manner (Fig. 6*A*). Half-maximal effect of protection against N2A cell death was obtained at a concentration of 0.5 μM AR-A014418, and the maximal effect was seen at 50 μM AR-A014418. A corresponding increase in cell survival was observed (Fig. 6*A*, *right panel*). Fluorescent microscopy was used to quantify the live (*green*) and dead (*red*) cells (Fig. 6*A*, *photos A–H*).

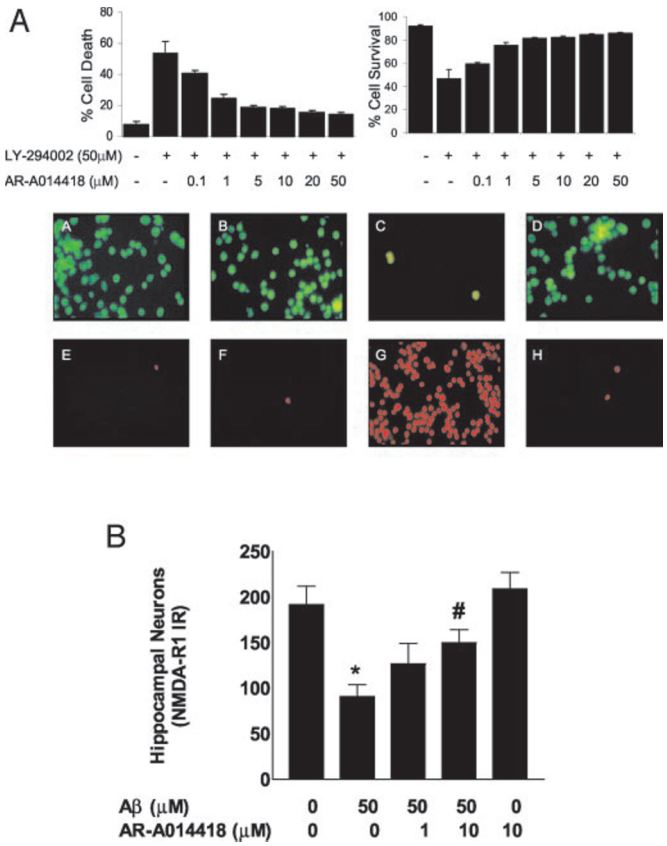

FIG. 6. **AR-A014418 inhibits neuronal cell death.** *A*, N2A cells were cultured for 2 days *in vitro* and then treated with LY-294002 in the presence of AR-A014418 or vehicle (Me_2SO) for 24 h. Viable and dead cells were stained with calcein AM and propidium iodide as described under "Experimental Procedures" and photographed at a fluorescence microscope. Percentages of specific cell death were determined as described under "Experimental Procedures." The data represent mean values ± S.E. of three different experiments performed in triplicate. AR-A014418 inhibits cell death with an IC_{50} value of 0.5 μM. Representative data are shown. *Subpanels A* and *E*, control; *B* and *F*, treated with AR-A014418; *C* and *G*, treated with LY-294002; *D* and *H*, treated with both AR-A014418 and LY-294002. *A–D* were stained with calcein (live cells), and *E–H* were stained with propidium iodide (dead cells). *B*, hippocampal organotypic slices were incubated in the absence (*Control*) or in the presence of Aβ 25–35 and 1 and 10 μM AR-A014418. After the different treatments, the number of NMDA-R1 immunoreactive pyramidal cells were counted as described under "Experimental Procedures." The average of three separate determinations is indicated. *, $p < 0.05$ compared with control. #, $p < 0.05$ compared with Aβ 25–35 alone.

Aβ Toxicity in Hippocampal Neurons—Exposure of cortical and hippocampal primary neuronal cultures to Aβ has been shown to induce activation of GSK3β (18) and cell death (19–21). Therefore, we determined the effect of GSK3β inhibition on Aβ-induced neurodegeneration in an organotypic culture system. In this system, Aβ exposure (50 μM for 4 days) results in a 44% decrease in the number of immunoreactive pyramidal shaped cells, as compared with control cultures. Incubation with 10 μM AR-A014418 significantly reduced (by more than 50%) the neuronal loss observed in the organotypic culture (Fig. 6*B*). At these concentrations, AR-A014418 by itself did not affect neuronal viability.

DISCUSSION

We report the identification and characterization of a small molecule that is a novel selective inhibitor of GSK3 catalytic activity. AR-A014418 is a thiazole identified in a high-throughput biochemical screen by using purified recombinant GSK3.

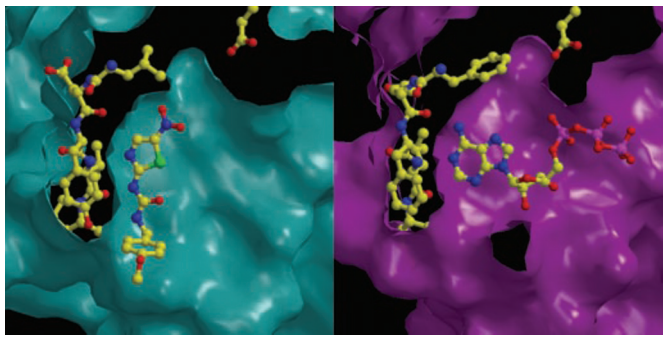

FIG. 7. **Surface representation of the ATP pocket of GSK3β-AR-A014418 (in *cyan*), and that of cdk2-ATP (*magenta*).**

AR-A014418 is unique because most reported GSK3β inhibitors are powerful cdk inhibitors (39), which is not the case for this compound. Additionally, we demonstrate here that AR-A014418 is specific against GSK3 in a panel of 26 kinases.

To investigate the mechanism of AR-A014418 inhibition, we have studied the substrate dependence of the kinase activity in the presence of the inhibitor. The data indicate that AR-A014418 has no effect on the V_{max} using ATP as substrate, confirming that AR-A014418 inhibits GSK3β by competing with ATP. Because the majority of the protein kinase inhibitors bind to the ATP pocket, we have resolved the crystal structure of GSK3β with AR-A014418. The crystal structure shows that the inhibitor binds through three hydrogen bonds, to the backbone atoms of Val-135 (both the amide N and the carbonyl O), a residue located in the hinge/linker region alongside of the ATP-binding pocket of the enzyme. The crystal structure of GSK3β in complex with AR-A014418 reveals the interactions formed and provides an explanation for its selectivity, providing invaluable information for the design of future lines of GSK3 inhibitors.

The structural basis for the selectivity of AR-A014418 against GSK3 with respect to cdk2 is shown in Fig. 7. The pictures depicted are surface representation of the ATP pocket of GSK3β-AR-A014418 (in *cyan*), and that of cdk2-ATP (in *magenta*, phosphorylated in complex with cyclin A (Protein Data Bank code 1qmz)). Overall, GSK3β has a more elongated pocket along the hinge/linker region, whereas cdk2 has a more compacted center region but with a wider opening in the entrance; in addition, the surface is more "hilly" (not as flat as in GSK3β). The so-called selectivity residue is different in the two structures, Leu-132 in GSK3β and Phe-80 in cdk2. The lining of the pocket in GSK3β is more flat than in cdk2 (most likely attributed to the difference Cys-199 in GSK3β/Ala-144 in cdk2). Furthermore, there is a significant difference in the entrance area of the ATP pocket. There is a salt bridge (Glu-Arg) in GSK3β that defines the boundary of the ATP pocket. The equivalent residues involved in the salt bridge become Gln-85 and Lys-89 in cdk2, where they take an anti-parallel relative orientation to each other. This Lys-89 actually points inwards to the ATP pocket, interacting to a main chain atom (carbonyl O of Ile-10) from the Gly-rich loop. The difference between Pro-136 (His-84 in cdk2) may also contribute to the formation of the salt bridge in GSK3β. Therefore, there is a wider opening in the entrance of the ATP pocket in cdk2.

The structural basis for the selectivity against cdk2 observed for AR-A014418 can partly be attributed to the differences in the entrance region of the ATP pocket. In GSK3β, the phenyl group fits well in this area. However, if this inhibitor would bind to cdk2, the side chain of Lys-89 would interfere with phenyl group, or even if this Lys would swing away to accommodate the inhibitor, there would be no favorable interactions with AR-A014418 as observed in the case of GSK3β. Alternatively, the position of the so-called selectivity residue, Phe-80 in cdk2, may have more tight unfavorable contact with the nitro group of the inhibitor if AR-A014418 would bind. The planar shape of the NO_2-thiazole part fits well and is favorable for interactions in the Cys-199 area of GSK3β. Another significant difference is that the polar interactions to the NO_2-thiazole part of AR-A014418 to the Lys-Asp salt bridge are mediated via a water molecule in GSK3β, whereas in the cdk2 the NO_2-salt bridge distance appears to be significantly shorter and the polar interaction would be direct, and not mediated via a water molecule.

The importance of AR-A014418 as a specific GSK3 inhibitor was validated by its capacity to interfere with two of the regulated processes playing an important role in AD: tau phosphorylation and β-amyloid-induced toxicity. GSK3β has been shown to phosphorylate tau in some of those sites that are hyperphosphorylated in PHFs, both in transfected cells (13) and *in vivo* (14, 15). As expected, from its ability to inhibit GSK3, AR-A014418 inhibited tau phosphorylation in cells overexpressing tau protein in a dose-dependent manner. GSK3 has been reported to play a role in the toxic effect mediated by β-amyloid, a protein that aggregates as extracellular amyloid plaques in AD brain. Exposure of cortical and hippocampal primary neuronal cultures to β-amyloid induces activation of GSK3β (18), tau hyperphosphorylation (19, 45), and cell death (19, 20). Blockade of GSK3β expression by antisense oligonucleotides (20) or its activity by lithium addition (21) inhibits β-amyloid-induced neurodegeneration of cortical and hippocampal primary cultures. Tau protein is essential to β-amyloid-induced neurotoxicity because hippocampal neurons cultured from tau knockout mice, treated with fibrillar β-amyloid, do not degenerate (46). In the current study, we demonstrate that AR-A014418 is able to inhibit tau phosphorylation as well as β-amyloid-induced neuronal death.

The PI3K/PKB signaling pathway is recognized as playing a central role in the survival of diverse cell types. GSK3 is one of several known substrates of PKB (47). PKB phosphorylates GSK3 in response to insulin and growth factors, which inhibits GSK3 activity and leads to the modulation of multiple GSK3-regulated cellular processes (47). We show that AR-A014418 protect cultured N2A cells from death induced by blocking PI3K/PKB pathway. The inhibition of neuronal death mediated by AR-A014418 correlates with inhibition of GSK3 activity, a principal regulatory target of the PI3K/PKB neuronal survival pathway (47).

In summary, AR-A014418 is an important research tool inasmuch as, at concentrations that AR-A014418 is able to inhibit GSK3 activity, this compound did not affect the activity of other 26 protein kinases tested, and especially does not inhibit cdc2 and cdk5, two GSK3-related kinases that are inhibited by published GSK3 inhibitors. Furthermore, AR-A014418 constitutes a lead compound with therapeutic potential for the treatment of AD, as well as other neurodegenerative disorders.

Acknowledgments—We thank Professor Philip Cohen (MRC Protein Phosphorylation Unit, University of Dundee, Dundee, Scotland, United Kingdom) for providing recombinant GSK3 and the selectivity screen for the various kinases and I. Janssen, C. Dartsch, and R. Svensson (AstraZeneca Biotech Laboratories, Gärtuna, Sweden).

REFERENCES

1. Alzheimer, A. (1911) *Z. Gesamte Neurol. Psychiat.* **4,** 356–385
2. Yankner, B. A. (1996) *Neuron* **16,** 921–932
3. Braak, H., and Braak, E. (1991) *Acta Neuropathol. (Berl.)* **82,** 239–259
4. Avila, J. (2000) *FEBS Lett.* **476,** 89–92
5. Goedert, M., and Spillantini, M. G. (2001) *Biochem. Soc. Symp.* **67,** 59–71
6. Lee, V. M., Goedert, M., and Trojanowski, J. Q. (2001) *Annu. Rev. Neurosci.* **24,** 1121–1159
7. Ishiguro, K., Shiratsuchi, A., Sato, S., Omori, A., Arioka, M., Kobayashi, S., Uchida, T., and Imahori, K. (1993) *FEBS Lett.* **325,** 167–172
8. Woodgett, J. R. (1990) *EMBO J.* **9,** 2431–2438

9. Hanger, D. P., Hughes, K., Woodgett, J. R., Brion, J. P., and Anderton, B. H. (1992) *Neurosci. Lett.* **147,** 58–62
10. Takahashi, M., Tomizawa, K., Kato, R., Sato, K., Uchida, T., Fujita, S. C., and Imahori, K. (1994) *J. Neurochem.* **63,** 245–255
11. Shiurba, R. A., Ishiguro, K., Takahashi, M., Sato, K., Spooner, E. T., Mercken, M., Yoshida, R., Wheelock, T. R., Yanagawa, H., Imahori, K., and Nixon, R. A. (1996) *Brain Res.* **737,** 119–132
12. Pei, J. J., Braak, E., Braak, H., Grundke-Iqbal, I., Iqbal, K., Winblad, B., and Cowburn, R. F. (1999) *J. Neuropathol. Exp. Neurol.* **58,** 1010–1019
13. Lovestone, S., Reynolds, C. H., Latimer, D., Davis, D. R., Anderton, B. H., Gallo, J. M., Hanger, D., Mulot, S., Marquardt, B., Stabel, S., *et al.* (1994) *Curr. Biol.* **4,** 1077–1086
14. Hong, M., Chen, D. C., Klein, P. S., and Lee, V. M. (1997) *J. Biol. Chem.* **272,** 25326–25332
15. Munoz-Montano, J. R., Moreno, F. J., Avila, J., and Diaz-Nido, J. (1997) *FEBS Lett.* **411,** 183–188
16. Grundke-Iqbal, I., Iqbal, K., Tung, Y. C., Quinlan, M., Wisniewski, H. M., and Binder, L. I. (1986) *Proc. Natl. Acad. Sci. U. S. A.* **83,** 4913–4917
17. Lee, V. M., Balin, B. J., Otvos, L., Jr., and Trojanowski, J. Q. (1991) *Science* **251,** 675–678
18. Takashima, A., Noguchi, K., Michel, G., Mercken, M., Hoshi, M., Ishiguro, K., and Imahori, K. (1996) *Neurosci. Lett.* **203,** 33–36
19. Busciglio, J., Lorenzo, A., Yeh, J., and Yankner, B. A. (1995) *Neuron* **14,** 879–888
20. Takashima, A., Noguchi, K., Sato, K., Hoshino, T., and Imahori, K. (1993) *Proc. Natl. Acad. Sci. U. S. A.* **90,** 7789–7793
21. Alvarez, G., Munoz-Montano, J. R., Satrustegui, J., Avila, J., Bogonez, E., and Diaz-Nido, J. (1999) *FEBS Lett.* **453,** 260–264
22. Takashima, A., Murayama, M., Murayama, O., Kohno, T., Honda, T., Yasutake, K., Nihonmatsu, N., Mercken, M., Yamaguchi, H., Sugihara, S., and Wolozin, B. (1998) *Proc. Natl. Acad. Sci. U. S. A.* **95,** 9637–9641
23. Yu, G., Chen, F., Levesque, G., Nishimura, M., Zhang, D. M., Levesque, L., Rogaeva, E., Xu, D., Liang, Y., Duthie, M., St. George-Hyslop, P. H., and Fraser, P. E. (1998) *J. Biol. Chem.* **273,** 16470–16475
24. Murayama, M., Tanaka, S., Palacino, J., Murayama, O., Honda, T., Sun, X., Yasutake, K., Nihonmatsu, N., Wolozin, B., and Takashima, A. (1998) *FEBS Lett.* **433,** 73–77
25. Zhang, Z., Hartmann, H., Do, V. M., Abramowski, D., Sturchler-Pierrat, C., Staufenbiel, M., Sommer, B., van de Wetering, M., Clevers, H., Saftig, P., De Strooper, B., He, X., and Yankner, B. A. (1998) *Nature* **395,** 698–702
26. Hoshi, M., Takashima, A., Noguchi, K., Murayama, M., Sato, M., Kondo, S., Saitoh, Y., Ishiguro, K., Hoshino, T., and Imahori, K. (1996) *Proc. Natl. Acad. Sci. U. S. A.* **93,** 2719–2723
27. Leroy, K., Boutajangout, A., Authelet, M., Woodgett, J. R., Anderton, B. H., and Brion, J. P. (2002) *Acta Neuropathol.* (*Berl.*) **103,** 91–99
28. Bhat, R. V., Shanley, J., Corell, M. P., Fieles, W. E., Keith, R. A., Scott, C. W., and Lee, C. M. (2000) *Proc. Natl. Acad. Sci. U. S. A.* **97,** 11074–11079
29. Hetman, M., Cavanaugh, J. E., Kimelman, D., and Xia, Z. (2000) *J. Neurosci.* **20,** 2567–2574
30. Salinas, P. C., and Hall, A. C. (1999) *Bipolar Disord.* **1,** 87–90
31. Lucas, J. J., Hernandez, F., Gomez-Ramos, P., Moran, M. A., Hen, R., and Avila, J. (2001) *EMBO J.* **20,** 27–39
32. Otvos, L., Jr., Feiner, L., Lang, E., Szendrei, G. I., Goedert, M., and Lee, V. M. (1994) *J. Neurosci. Res.* **39,** 669–673
33. Hernandez, F., Borrell, J., Guaza, C., Avila, J., and Lucas, J. J. (2002) *J. Neurochem.* **83,** 1529–1533
34. Jackson, G. R., Wiedau-Pazos, M., Sang, T. K., Wagle, N., Brown, C. A., Massachi, S., and Geschwind, D. H. (2002) *Neuron* **34,** 509–519
35. Coghlan, M. P., Culbert, A. A., Cross, D. A., Corcoran, S. L., Yates, J. W., Pearce, N. J., Rausch, O. L., Murphy, G. J., Carter, P. S., Roxbee Cox, L., Mills, D., Brown, M. J., Haigh, D., Ward, R. W., Smith, D. G., Murray, K. J., Reith, A. D., and Holder, J. C. (2000) *Chem. Biol.* **7,** 793–803
36. Hers, I., Tavare, J. M., and Denton, R. M. (1999) *FEBS Lett.* **460,** 433–436
37. Smith, D. G., Buffet, M., Fenwick, A. E., Haigh, D., Ife, R. J., Saunders, M., Slingsby, B. P., Stacey, R., and Ward, R. W. (2001) *Bioorg. Med. Chem. Lett.* **11,** 635–639
38. Meijer, L., Thunnissen, A. M., White, A. W., Garnier, M., Nikolic, M., Tsai, L. H., Walter, J., Cleverley, K. E., Salinas, P. C., Wu, Y. Z., Biernat, J., Mandelkow, E. M., Kim, S. H., and Pettit, G. R. (2000) *Chem. Biol.* **7,** 51–63
39. Leclerc, S., Garnier, M., Hoessel, R., Marko, D., Bibb, J. A., Snyder, G. L., Greengard, P., Biernat, J., Wu, Y. Z., Mandelkow, E. M., Eisenbrand, G., and Meijer, L. (2001) *J. Biol. Chem.* **276,** 251–260
40. Martinez, A., Alonso, M., Castro, A., Perez, C., and Moreno, F. J. (2002) *J. Med. Chem.* **45,** 1292–1299
41. Davies, S. P., Reddy, H., Caivano, M., and Cohen, P. (2000) *Biochem. J.* **351,** 95–105
42. Mattson, M. P., Barger, S. W., Begley, J. G., and Mark, R. J. (1995) *Methods Cell Biol.* **46,** 187–216
43. Klein, P. S., and Melton, D. A. (1996) *Proc. Natl. Acad. Sci. U. S. A.* **93,** 8455–8459
44. Vlahos, C. J., Matter, W. F., Hui, K. Y., and Brown, R. F. (1994) *J. Biol. Chem.* **269,** 5241–5248
45. Ferreira, A., Lu, Q., Orecchio, L., and Kosik, K. S. (1997) *Mol. Cell. Neurosci.* **9,** 220–234
46. Rapoport, M., Dawson, H. N., Binder, L. I., Vitek, M. P., and Ferreira, A. (2002) *Proc. Natl. Acad. Sci. U. S. A.* **99,** 6364–6369
47. Cohen, P., and Frame, S. (2001) *Nat. Rev. Mol. Cell. Biol.* **2,** 769–776
48. Studer, L., Spenger, C., Luthman, J., Seiler, R. W. (1994) *J. Comp. Neurol.* **340,** 281–296
49. Luthman, J., Radesäter, A.-C., and Öberg, C. (1998) *Amino Acids* **14,** 263–269
50. Cheng, Y., and Prusoff, W. (1973) *Biochem. Pharmacol.* **22,** 3099–3108
51. Phiel, C. J., Wilson, C. A., Lee, V. M., and Klein, P. S. (2003) *Nature* **423,** 435–439
52. Laskowski, R., MacArthur, M. W., Moss, D. S., and Thornton, J. M. (1993) *J. Appl. Crystallogr.* **26,** 283–291